Synergy of two lower hybrid waves with different frequencies on EAST

X M Zhai[1,2,3], J L Chen[1,3,a)], N Xiang[1,3,a)], P T Bonoli[4] and S Shiraiwa[4]

[1] *Institute of Plasma Physics, Chinese Academy of Sciences, Hefei 230031, China*

[2] *University of Chinese Academy of Sciences，Beijing 100049, China*

[3] *Center for Magnetic Fusion Theory, Chinese Academy of Sciences, Hefei 230031, China*

[4] *Plasma Science and Fusion Center, Massachusetts Institute of Technology, Cambridge, Massachusetts, 02139 USA*

Lower hybrid current drive (LHCD) is one of the major approaches maintaining long pulse discharges on EAST. There are two lower hybrid (LH) systems on EAST launching waves at 4.6 GHz and 2.45 GHz into the plasma, respectively, and the input power of 4.6 GHz wave is typically dominant. In this work the synergy of the two waves and the modification of the power deposition of the 4.6 GHz wave by coupling the 2.45 GHz wave are investigated theoretically. According to the phase space analysis, the wave propagation domains of the two LH waves are always overlapping substantially with each other for typical LHCD experimental parameters on EAST, indicating that the coupling between them might be strong. Ray-tracing/Fokker-Planck simulations for a LH current drive experiment on EAST show that the change of the power deposition profile due to the coupling could be understood by the rise and fall of the tails of the parallel electron distribution functions on different flux surfaces. If either the injected wave power at 2.45 GHz is comparable with that at 4.6 GHz or the incident $N_{\|}$ of the 2.45 GHz wave reaches a high value (e.g., $5.7/\sqrt{T_{e,0}}$), the power deposition profile of the 4.6 GHz wave can be modified greatly due to the coupling with the 2.45 GHz wave. With the parameters compatible with the ability of LH wave system on EAST, injection of the 2.45 GHz wave can still modify the power deposition profile of the 4.6 GHz wave significantly by combining those two approaches. Finally it is shown how a 4.6 GHz wave which cannot be Landau damped when injected alone is absorbed in low density plasmas with magnetic shear reversal configuration in the presence of a 2.45 GHz wave.

[a)] Electronic mails: chen@ipp.ac.cn; xiangn@ipp.ac.cn

I. INTRODUCTION

Lower hybrid current drive (LHCD) plays an important role not only in driving current effectively,[1] but also in controlling current profiles, which is crucial for development of advanced scenarios in tokamaks.[2-5] The current profile control by LHCD has been demonstrated in the pioneer experiments on Tore Supra[6] and JT-60U[7]and recently on EAST.[8] The special condition for experiments on EAST is that there are two lower hybrid (LH) systems launching waves at 4.6 GHz and 2.45 GHz into the plasma, respectively, and the input power of 4.6 GHz wave is typically dominant. The combinations of radio frequency (rf) waves at different launched frequencies have been investigated intensively. The two main types of the combinations are that of electron cyclotron (EC) waves and LH waves and that of two LH waves. The synergy between electron cyclotron (EC) waves and LH waves has been demonstrated experimentally,[9] numerically[10-12] and analytically.[13, 14] Meanwhile, the combination of LH waves has motivated experimental researches on the synergistic effect on different machines.[15-18] The synergy between two LH waves is the concern of this work.

It has been reported that the synergy of two LH waves with different spectra of parallel refractive index $N_{\parallel}$ (to the applied magnetic field $\vec{B}$) was responsible for the improvement of the current drive efficiency and the modification of the current profile, which was indicated by the change of hard X-ray emission signals and internal inductance l_i.[15, 17] The key physical mechanism accounting for the 'local' synergistic effect has been identified in previous works with the solution of quasi-linear Fokker-Planck equation (e.g., Ref. 19), which, in short, is the formation of velocity-space plateau on the parallel electron distribution function $f\left(v_{\parallel}\right)$ by the low phase velocity wave increases the number of fast electrons resonant with the high phase velocity wave. The synergistic effect is sensitive to the relative distance between the resonance regions of the two waves. Within an ideal model the effect could be estimated analytically by the parameter of synergy factor under the assumption that the wave fields for the two waves are strong enough to make two plateaus at the same time.[20] However, these analyses are insufficient to figure out how the synergy affects the power deposition profile, the total power absorption and the current drive efficiency. These analyses did not provide a prediction that can be easily observed in experiment such as the hard X-ray energy spectra (e.g., Fig. 4 in Ref. 15). Only based on these analyses it is still very difficult to figure out the possibility of controlling the power

deposition of the main wave (4.6 GHz) by the simultaneous injection of the auxiliary wave (2.45 GHz) on EAST. The phase space "engineering" with experimental parameters is essential to deal with the above issues.

More specifically the wave kinematics/dynamics in phase space should be evaluated together with the solution of quasi-linear Fokker-Planck equation. In this work we apply the phase space analytic technique for the propagation domain (i.e., wave kinematics) to give a general analysis on the strength of the coupling between the two LH waves and use ray-tracing simulations for wave dynamics (coupled with a Fokker-Planck solver) to do the detailed research on special cases. The type of phase space engineering[21] could be extremely valuable in applications where improvement of current drive efficiency and more precise control of the LH wave deposition are required, such as controlling the position of shear reversal in plasmas with internal transport barriers, or in the control of neoclassical tearing modes, for example.

A reversed shear experiment sustained mainly by 4.6 GHz LH waves on EAST is selected as a 'baseline' in this work. The power deposition of the 4.6 GHz wave was localized and off axis, which can be interpreted by the phase space analysis as shown in Ref. 22, while the power deposition of the 2.45 GHz wave was broad. Since the power of the 4.6 GHz wave was much larger that of the 2.45 GHz wave in the experiment, the synergy effect was weak and could be ignored, which was confirmed by the quantitative comparison between the contributions of the different frequency waves to the total power deposition (See Appendix B in Ref. 22). Therefore, the condition of that experiment is a good reference for studying on the synergy between the two LH waves within an extended parameter regime and figuring out how the power deposition of the 4.6 GHz wave could be broadened by the coupling with 2.45 GHz wave.

The paper is organized as follows. In Section II, the overlapping of wave propagation domains of the 2.45 GHz and 4.6 GHz LH waves is estimated by the phase space analytic technique for typical parameters on EAST. In Section III, we will show some quasi-linear simulation results not only to demonstrate the synergy between the two waves but also to investigate how the power deposition profile of the 4.6 GHz wave can be modified by coupling the 2.45 GHz wave. In Section IV, it is demonstrated that the coupling of the two waves could yield significant enhancement on the total power deposition rate of the 4.6 GHz wave. The summary is given in Section V.

II. OVERLAPPING OF WAVE PROPAGATION DOMAINS OF 2.45 GHZ AND 4.6 GHZ WAVES

The theoretical analysis for the synergy between two LH waves has shown that the distance between the resonance regions raised by each wave and the height of the velocity-space plateau in the electron velocity distribution function play key roles in synergy.[20] When extending the local analysis to the whole plasma radius, the range of parallel refractive index $N_{\|}$ could be roughly estimated by the phase space technique as follows. The largest and lowest values of $N_{\|}$ (denoted as boundaries of wave propagation domain) subject to the wave dispersion relation in cold plasma limit can be estimated as[22-25]

$$N_{\|}=\frac{N_{\varphi,\mathrm{axis}}}{\left(1\mp\sqrt{\alpha}\sqrt{n_e}\,B_\theta/B\right)},$$

where '-' and '+' give the upper and lower boundaries on parallel (to the total magnetic field $\vec{B}$) refractive index $N_{\|}$, and $\alpha\equiv\omega_{pe}^2/S\omega^2 n_e$. S is the terms of the Stix cold plasma dielectric tensor.[26] ω_{pe} is the electron plasma frequency and ω is the LH wave frequency. n_e is the plasma density. $N_{\varphi,\mathrm{axis}}$ is the toroidal refractive index at the magnetic axis. B_θ is the poloidal magnetic field. The overlapping of the wave propagation domains between two LH waves mainly relies on the plasma parameters, such as the ratio of poloidal magnetic field over total magnetic field B_θ/B, plasma density n_e and launched $N_{\|}$. The wave propagation domains can be separated, attached and overlapped with each other depending on different value of the above parameters. For the typical parameters on EAST, the wave propagation domains in the phase space are always overlapping substantially with each other, e.g., as shown in Figure 1, which motivates us to explore whether there would be strong coupling effect in the combined LH waves experiments on EAST. In this work only the waves in the main lobes of the launched spectra are analyzed.

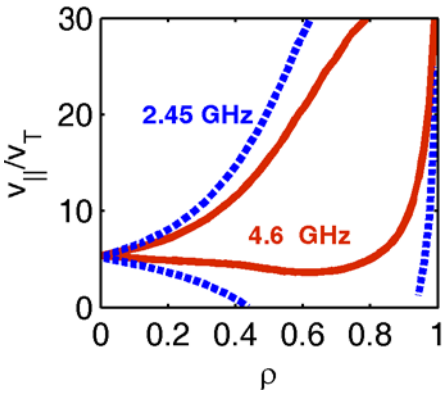

Figure 1. The wave propagation domains for the 2.45 GHz and 4.6 GHz waves on EAST. The ratio of parallel phase velocity and local thermal velocity of electron is defined as $v_{\|}/v_T \equiv c/\left(N_{\|}v_T\right)$,where c is the light speed and $v_T \equiv \sqrt{T_e/m_e}$. The main parameters are based on those of the EAST discharge 63982. The incident $N_{\|}$ for 4.6 GHz and 2.45 GHz is 2.04 and 2.1, respectively.

III. POWER DEPOSITION MODIFICATIONS DUE TO THE COUPLING BETWEEN TWO WAVES

The combined ray-tracing and Fokker-Planck simulation packages are widely used to calculate the quasilinear electron distribution function that is consistent with the local wave damping, which have been used successfully for the LHCD modeling in many tokamaks.[2, 27] GENRAY/CQL3D is one of these packages and has been routinely used to analyze LHCD on EAST,[22, 28, 29] Alcator C-Mod[30, 31] and synergistic effects between LH and EC waves.[32] In this work we use GENRAY/ to study the synergy between the 2.45 GHz and 4.6 GHz LH waves. More specifically, CQL3D is used to solve the bounce-averaged quasilinear Fokker-Planck equation for the electron and no fast electron radial diffusion effect is considered in the simulations for simplicity.

The coupling effect on modification of power deposition profiles for both of the two waves is our primary concern in this section. The main parameter setting in the simulations is based on the experimental data of the L-mode discharge 63982 in the 2016 campaign of EAST, which is a fully non-inductive LHCD discharge.[8] The total injected LH wave power is about 2 MW and the ratio of the injected power at 4.6 GHz ($P_{4.6}$) over that at 2.45 GHz ($P_{2.45}$) is about 4/1. The peak $N_{\|}$ of the main lobe in the launched spectra for 4.6 GHz and 2.45 GHz is 2.04 and 2.1, respectively. In the simulations the numbers of rays are large enough to obtain the stable simulation results. The profiles of electron

density n_e, temperature T_e and safety factor q are shown in Figure 2.

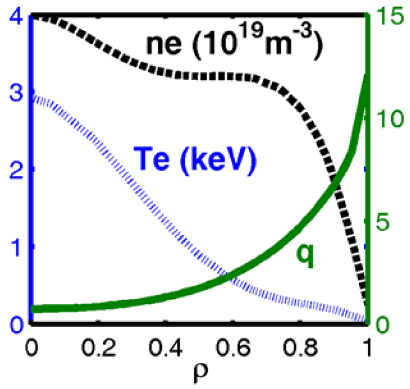

Figure 2. The profiles of electron density, temperature and safety factor of the shot 63982 at t~5s. The abscissa for the radial coordinate ρ is the square root of normalized toroidal magnetic flux.

A. Power deposition profiles with and without coupling

The comparisons of power deposition of the 2.45 GHz wave with and without the coupling with the 4.6 GHz wave are illustrated in Figure 3. When the 2.45 GHz wave is launched alone, the peak value of its power deposition profile locates at the flux surface ρ=0.2 . In contrast, its wave power is mainly deposited in the off-axis region $\rho \sim 0.6$ when the 4.6 GHz wave is injected simultaneously. This is a clear demonstration of the strong coupling between the two LH waves.

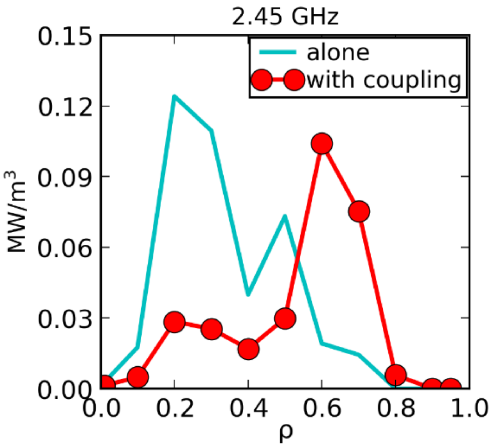

Figure 3. Power deposition profiles of the 2.45 GHz wave as it is injected alone (cyan solid line) and as it is coupled with the 4.6 GHz wave (red solid line and circle marker). The coupled one is extracted from the CQL3D output data when the two waves are coupled in the simulation.

The significant modification of power deposition at ρ=0.6 can be interpreted by the deformation of parallel electron velocity distribution function *f* (defined as the integral of the electron distribution function f_e over perpendicular velocity $v_\perp$, i.e., $\int_0^\infty f_e\left(v_\perp, v_\parallel\right)v_\perp dv_\perp$). As shown in Figure 4, the resonant plateau height of the 2.45 GHz wave is much lower than that of the 4.6 GHz wave, indicating that much less electrons can interact resonantly with the 2.45 GHz wave and the 2.45 GHz wave is hardly damped. The simultaneous injection of the 4.6 GHz wave power leads to a pronounced rise of the resonant plateau compared to that with the 2.45 GHz wave alone and the power deposition of the 2.45 GHz wave is now significantly enhanced near ρ=0.6 as shown. According to the driven current densities calculated by CQL3D for the coupled injection case J_{coupled}, the 2.45 GHz wave injection alone $J_{2.45}$ and the 4.6 GHz wave injection alone $J_{4.6}$, the synergy factor $J_{\text{coupled}}/\left(J_{2.45}+J_{4.6}\right)$ (defined in Ref. 20) at this flux surface is about 1.2, indicating the synergy on this flux surface. By the way, the power deposition of the 2.45 GHz wave at $\rho \le 0.5$ is not enhanced by the coupling with the 4.6 GHz wave since few of resonant electron interacts with the 4.6 GHz wave in the region as speculated by the power deposition profile shown in Figure 5.

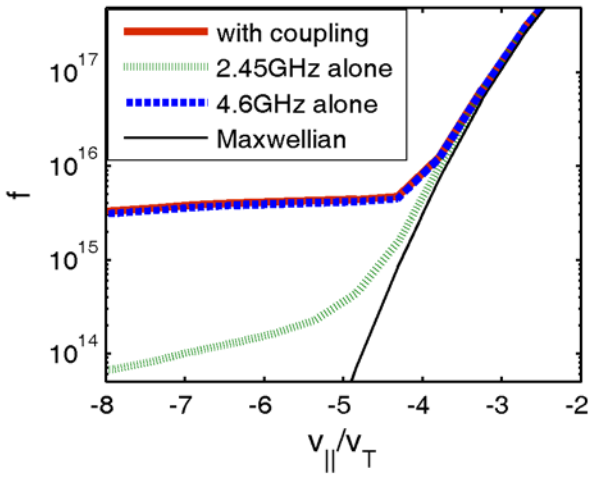

Figure 4. Parallel electron velocity distribution functions in the logarithmic scale versus the parallel phase velocity normalized by the local thermal velocity at ρ=0.6. The non-Maxwellian electron distribution function for the 2.45 GHz wave alone is denoted by the green dotted line, while the blue dashed line is for the 4.6 GHz wave alone in the uncoupled simulations. The non-Maxwellian distribution function for the coupled two waves is characterized by the red solid line. The thin solid line represents the background Maxwellian distribution.

The modification due to the coupling with the 2.45 GHz wave on power deposition profile of the

4.6 GHz wave is weak as shown in Figure 5. All the wave power of the 4.6 GHz wave with the coupling is almost deposited at the off-axis radial location as that without the coupling. Special attention should be paid to the change of power density in the core region $\rho \sim 0.2$, where the wave power of the 2.45 GHz wave alone is mainly deposited. We also check the electron distribution functions at ρ=0.2 to clarify this point.

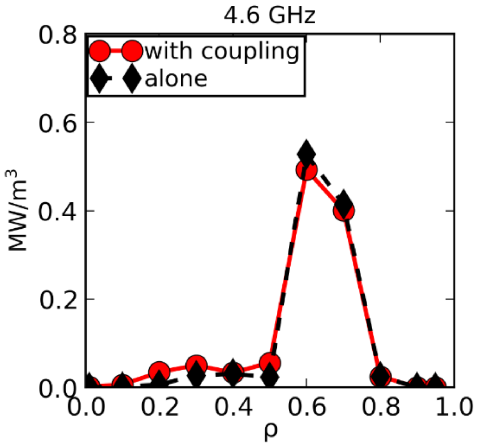

Figure 5. Power deposition profiles of the 4.6 GHz wave with (circle) and without (diamond) the coupling of the 2.45 GHz wave in CQL3D calculations.

Figure 6 shows the comparisons of f at ρ=0.2. The resonance region of the 4.6 GHz wave is totally covered by that of the 2.45 GHz wave, which agrees with the phase space analysis of overlapping in Section II. For the 4.6 GHz wave, the accessible lower limit of phase velocity of resonance region is about $5v_T$, which can be inferred from the phase space analysis and is independent of the detailed ray trajectories. Therefore the power deposition of the 4.6 GHz wave alone is weak here. Since the resonance region of the 2.45 GHz wave can reach the lower phase velocity and raise the plateau in the tail of f (from blue dash line to red solid line), its coupling with the 4.6 GHz wave increases the number of fast electron resonant with the 4.6 GHz wave and thus makes more wave power at 4.6 GHz be deposited. Since the power absorption of the 2.45 GHz wave at other flux surfaces (e.g. ρ~0.6) is enhanced by coupling the 4.6 GHz wave as demonstrated in Figure 3, the remaining power of the 2.45 GHz wave at $\rho \sim 0.2$ decreases and the enhancement on the power deposition of the 4.6 GHz wave due to the 2.45 GHz wave is limited. This is also illustrated in Figure 6 as the plateau for the coupled case is lower than that for the 2.45 GHz wave alone case.

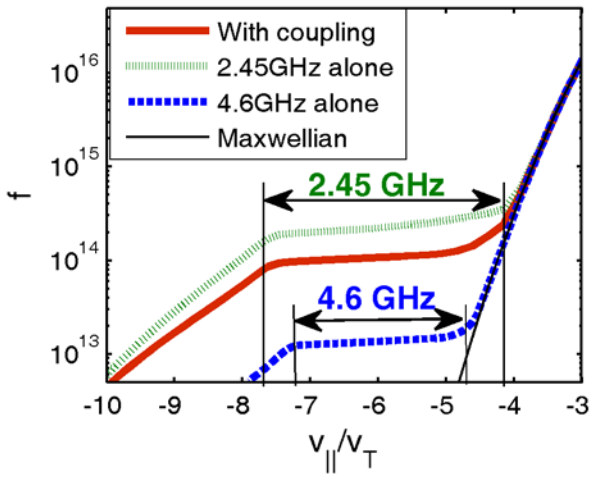

Figure 6. Parallel electron velocity distribution functions at ρ=0.2 . The notations for lines are the same as that in Figure 4. The resonance regions for the two waves are explicitly shown too.

B. Modify power deposition profile of the 4.6 GHz wave by injecting the 2.45 GHz wave simultaneously

Two approaches can possibly increase the number of fast electrons resonant with the 4.6 GHz wave at ρ=0.2 and enhance the modification of power deposition profile of the 4.6 GHz wave by coupling the 2.45 GHz wave. One is to increase the wave power of the 2.45 GHz wave reaching the region ρ~0.2 . The other one is to change the incident $N_{||}$ of the 2.45 GHz wave to make it yield the resonance region with lower phase velocity.

1. Increasing the power fraction of the 2.45 GHz wave

The numerical results of scanning the $P_{4.6}/P_{2.45}$ value while keeping the total injected wave power being about 2 MW are shown in Figure 7. The larger the power fraction of the 2.45 GHz wave, the greater the modification of the power deposition profile of the 4.6 GHz wave. When the wave power at 2.45 GHz increases to the level comparable with that at 4.6 GHz (i.e., $P_{4.6}/P_{2.45}=1.0:1.0$), the power density of the 4.6 GHz wave at ρ=0.2 has been remarkably enhanced. When the power of the 2.45 GHz wave is larger (i.e., $P_{4.6}/P_{2.45}=0.4:1.6$), it dominates and broadens the power deposition profile of the 4.6 GHz wave, which is clearly different from the case as the 4.6 GHz wave is injected alone.

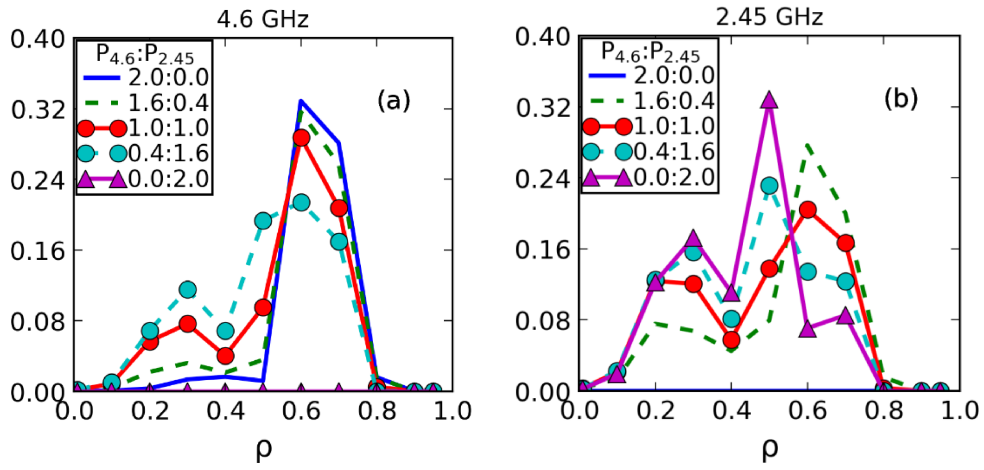

Figure 7. The normalized power deposition profiles for the 4.6 GHz (a) and 2.45 GHz (b) waves corresponding to different injected wave power when the two waves are coupled together. The total power is unchanged as $P_{4.6}+P_{2.45}$=2 MW . For illustrating the change of the shape of power deposition profile clearly, the power density is normalized by the injected power at each frequency.

2. Changing the incident $N_{||}$ of the 2.45 GHz wave

For the 2.45 GHz wave system on EAST, the launched $N_{||}$ of the main lobe could be up to 2.8. GENRAY/CQL3D simulations with increasing the incident $N_{||}$ of the 2.45 GHz wave in shot 63982 are performed with experimental power level, i.e., $P_{4.6}/P_{2.45}\approx 4/1$. As illustrated in Figure 8, the power deposition of the 2.45 GHz wave in the core region increases with the incident $N_{||}$ while it remains almost unaffected in the outer region ($\rho>0.5$). It is found that the plateau in the distribution function at ρ=0.2 moves toward the lower phase velocity, which could yield more electrons resonant with the 2.45 GHz wave, and make the single-pass power absorption of the 2.45 GHz wave stronger. As a result, the resonant electron numbers with the 4.6 GHz wave increases, the power deposition of the 4.6 GHz wave at the core plasma region shows a distinct enhancement and the profile is broadened. As $N_{||}=3.5$, the power deposition of the 2.45 GHz wave becomes near axis and the peak value of the power deposition profile of the 4.6 GHz wave in the near-axis region becomes comparable to that in the off-axis region as shown in Figure 8 (a). Hereinafter $T_{e,0}$ denotes the electron temperature in keV on the magnetic axis.

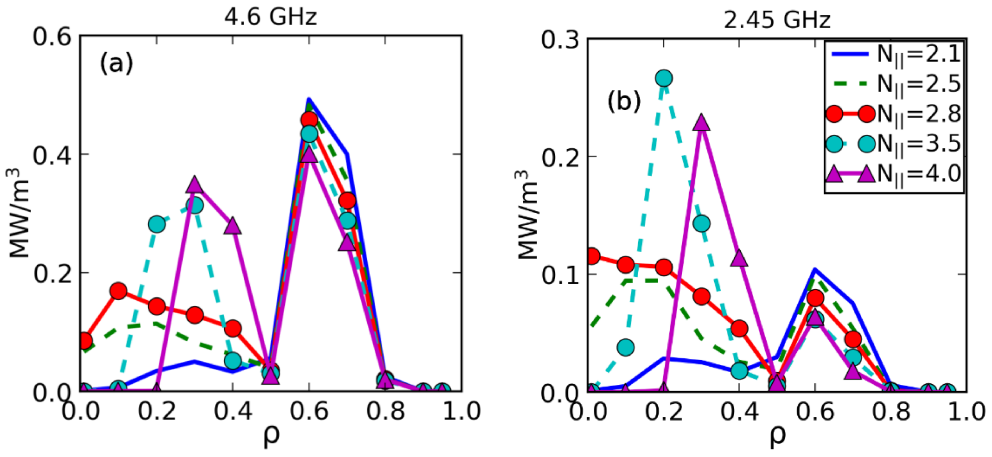

Figure 8. The power deposition profiles with changing the incident $N_{||}$ of the 2.45 GHz wave. (a) The 4.6 GHz wave and (b) the 2.45 GHz wave.

3. Application of a combined approach

Based on the previous analysis, significant modification on the power deposition of the 4.6 GHz wave could be accessed by properly increasing the injected wave power and the launched $N_{||}$ of the 2.45 GHz wave at the same time. For the parameters discussed in this section, the coupling effect between the two waves can be significant with $P_{4.6}/P_{2.45} = 1.25\ \text{MW}/0.75\ \text{MW}$ and the incident $N_{||}$ for the 2.45 GHz wave being 2.8. These parameters can be achieved within the present scope of the 2.45 GHz LH system in operation on EAST. As illustrated in Figure 9(a), the amplitude of power density for the 4.6 GHz wave in the radial region $\rho \le 0.4$ is significantly enhanced due to coupling with the 2.45 GHz wave, and is comparable with the peak value in the off-axis region. The power deposition profile is broadened.

In Figure 9(b), the simulated driven current profile with coupling is compared with the sum of those without coupling. The synergy factors are apparently larger than 1 in the core region $\rho \le 0.4$. Accordingly, the simulated total driven current in the coupled case is 15% larger than the sum of those in the uncoupled cases.

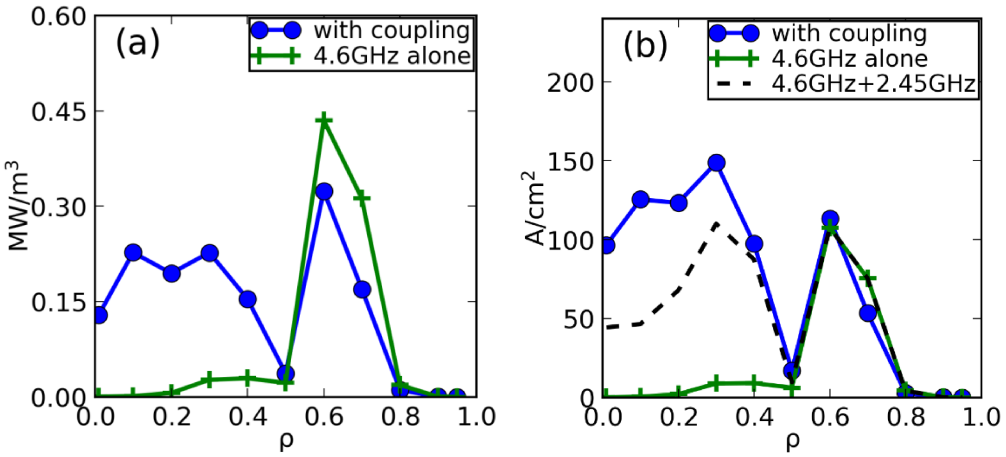

Figure 9. (a) The power deposition profiles of the 4.6 GHz wave with and without coupling with the 2.45 GHz wave. (b) The driven current profiles for the two waves injected together and the 4.6 GHz wave injected alone as well as the sum of the two waves as they are injected alone. $P_{4.6}/P_{2.45} = 1.25\ \text{MW} / 0.75\ \text{MW}$ and the incident $N_{\|}$ for the 2.45 GHz wave is 2.8.

The synergy could be proved by the change of the hard X-ray (HXR) energy spectra in experiments (e.g., Fig. 4 in Ref. 15 about experiments on JT-60U). The HXR energy spectra in the photon energy interval 20–200 keV are shown in Figure 10 from the synthetic diagnostics in the CQL3D simulations above. The spectra with the two waves injected simultaneously (blue solid line with closed circles) are obviously different from the sum of the spectra corresponding to the two waves injected alone (dashed line). The spectrum of channel 13 for the coupled case is larger than the sum of spectra by the two waves injected alone, which implies the number of fast electrons in the core region is increased by the coupling and can be a demonstration for the synergy. On the contrary, the spectrum of channel 19 for the coupled case is lower than the sum which implies the number of fast electrons in the plasma edge is decreased by the coupling.

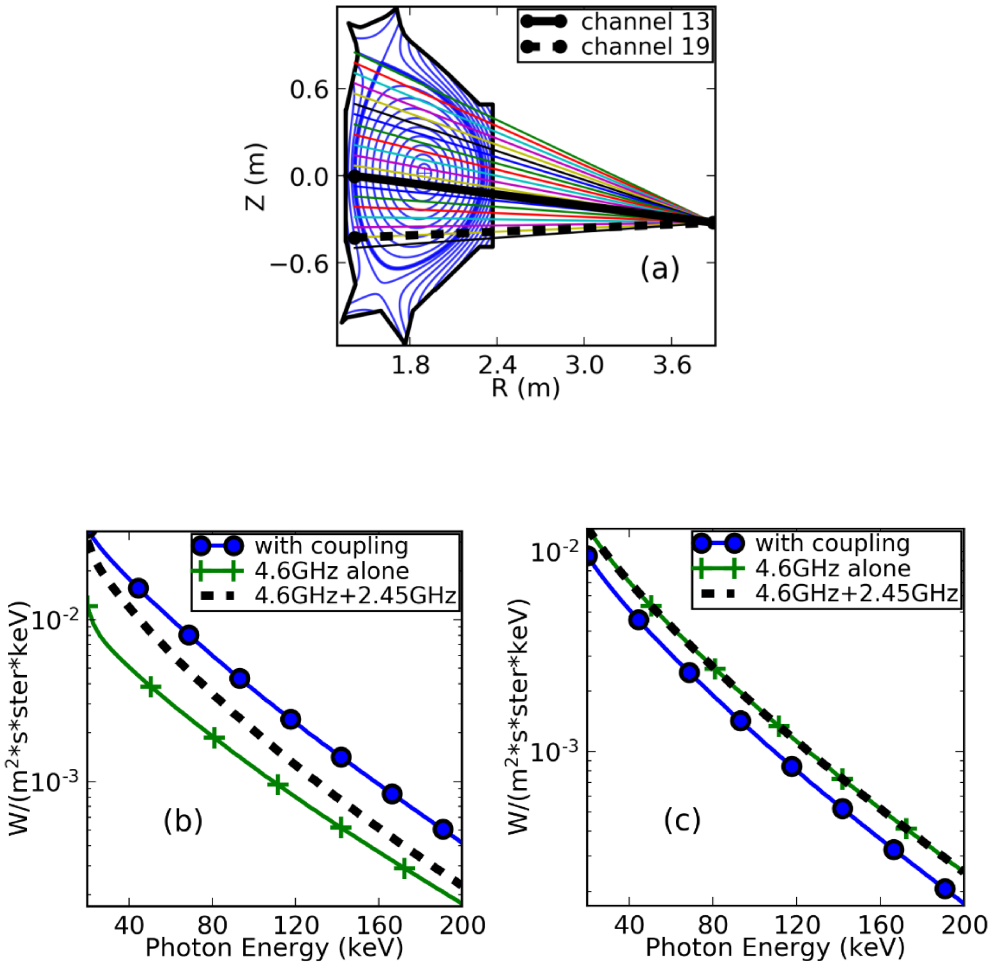

Figure 10. The HXR energy spectra for the two waves injected together, the 4.6 GHz wave injected alone and the sum of the two waves as they are injected alone. (a) The diagram of the viewing chords in poloidal cross-section for the HXR camera on EAST. (b) The HXR energy spectra at Channel 13 tangential to $\rho \sim 0.1$. (c) The HXR energy spectra at Channel 19 tangential to $\rho \sim 0.7$.

In conclusion, if either the injected wave power at 2.45 GHz is comparable with that at 4.6 GHz or the incident $N_{||}$ of the 2.45 GHz wave reaches the high value (e.g., $5.7/\sqrt{T_{e,0}}$), the power deposition profile of the 4.6 GHz wave can be modified greatly by coupling the 2.45 GHz wave. Within the ability of LH system on EAST, a significant modification on power deposition profile of the 4.6 GHz wave can still be accessed by combing these two approaches.

IV. ENHANCEMENT ON TOTAL POWER ABSORPTION

In the previous section the cases have been shown how the power deposition profile of an injected

4.6 GHz wave is affected by injecting a 2.45 GHz wave, where the 4.6 GHz wave itself can interact with electrons via Landau damping. In this section, we show that for a 4.6 GHz wave which cannot be Landau damped when injected alone, it can be absorbed in the plasma with the injection of a 2.45 GHz wave.

In magnetic shear reversal configuration plasmas but with low plasma density on EAST, the LH wave at 4.6 GHz would not deposit its power well if it is injected alone, while the wave power at 2.45 GHz can be always effectively absorbed. This is expected according to the wave propagation domain in the $(\rho, N_{\parallel})$ space as shown in Figure 11 (a). For typical parameters on EAST, the propagation domain for the 4.6 GHz LH wave is bounded in $N_{\parallel}$ space and that for the 2.45 GHz LH wave is unbounded.[22] Then the upper boundary of $N_{\parallel}$ for the 4.6 GHz LH wave (i.e., upper solid line in Figure 11 (a)) is finite and possibly much lower than that for strong electron Landau damping (ELD) condition over the whole radial region. Thus it is expected that the power absorption of the 4.6 GHz wave by Landau damping is bad in this situation.

Since the propagation domains of the two LH waves are significantly overlapping as shown in Figure 1, it is reasonable to infer that when the 4.6 GHz LH wave alone cannot damp well, its power absorption could be greatly enhanced over a broad radial region if the 2.45 GHz LH wave is launched simultaneously. This point is demonstrated in the simulations shown below.

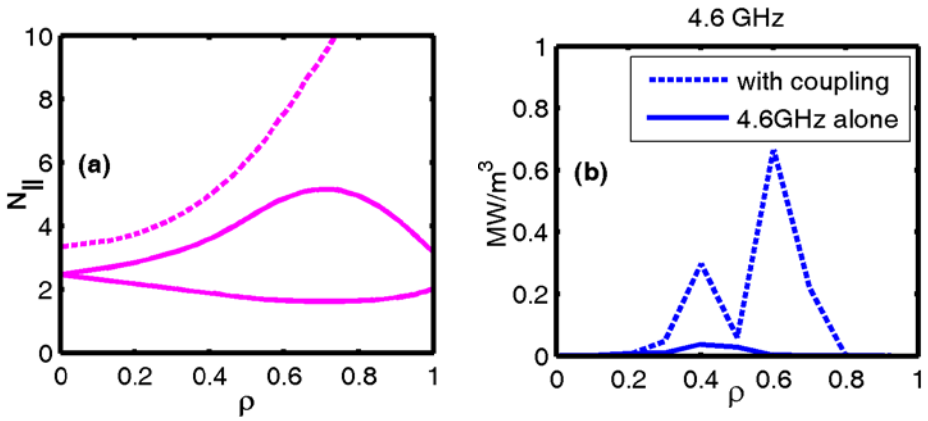

Figure 11. (a) Boundaries of wave propagation domain in phase space for the 4.6 GHz wave and (b) power deposition profiles of the 4.6 GHz wave with and without coupling to the 2.45 GHz wave in the EAST plasmas with reversed magnetic shear q profile and low electron density (i.e., scaling the density shown in Figure 2 by a factor of 0.4). The solid curves denote the boundaries of propagation domain for $N_{\parallel}$. The dashed curve at the top of (a) represents $N_{\parallel,\mathrm{L}}$ for the strong electron Landau damping condition $N_{\parallel,L} \sim 5.7/\sqrt{T_e}$. As $N_{\parallel}$ is upshifted

to satisfy the condition $v_{\|}/v_T = c/N_{\|}v_T = 3 \sim 5$, the LH waves can interact with enough resonant electrons and be absorbed significantly. Here we use the ratio $v_{\|}/v_T \sim 4$ to estimate $N_{\|,\mathrm{L}}$, and the GENRAY/CQL3D simulations for LH waves on EAST confirm that the wave is strongly damped as $v_{\|}/v_T$ gets close to 4. At the same time we refer the readers to a general derivation given in Ref. 33.

The parameter settings in the simulations are the same as those in the part (2) of Section III, except the experimental density profile is scaled by a factor of 0.4, which is in the scope of experimental density in EAST operation, e.g., that for the recent experiment achieving 10 keV. The injected power for the 4.6 GHz wave and the 2.45 GHz wave is 1.6 MW and 0.4 MW, respectively. Figure 11 (b) shows the simulated power deposition profiles of the 4.6 GHz wave with and without coupling to the 2.45 GHz wave. Without the coupling the power absorption rate (defined as the ratio of deposited power by Landau damping over injected power) for the 4.6 GHz wave is only 5%, which is consistent with the prediction by phase space analysis above. About 72% of the total injected power still cannot be deposited at the end of the simulations. This indicates that the 4.6 GHz wave should not be launched alone with these plasma parameters. In contrast, the power deposition rate for the 4.6 GHz wave is close to 100% with the coupling to the 2.45 GHz wave.

The parallel electron distribution functions for the above cases at ρ=0.6 are shown in Figure 12. There is a pronounced rise of *f* in the resonance region in the coupled case compared with that in the 4.6 GHz wave alone case. Notably the rise of fast electron in the range $-v_{\|}/v_T < 5.5$ is ascribed to the injection of the 2.45 GHz wave. This significant rise explains the enhancement on the power damping of the 4.6 GHz wave.

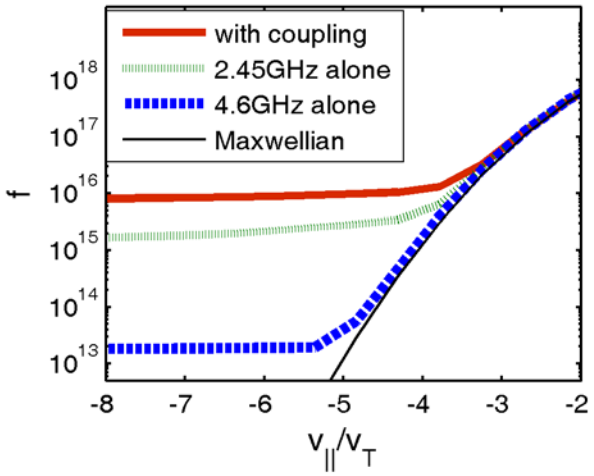

Figure 12. Parallel electron distribution functions at ρ=0.6 . The notations for lines are the same as that in Figure 4.

V. SUMMARY

The synergy between two LH waves on EAST and the modification of the power deposition of the 4.6 GHz wave by coupling the 2.45 GHz wave via phase space engineering are the concerns of this work. According to the phase space analysis, the wave propagation domains of the two LH waves are always overlapping substantially with typical parameters on EAST. Therefore the coupling between the 2.45 GHz and 4.6 GHz waves would be strong. Ray-tracing/Fokker-Planck simulations show that the change of the power deposition profile due to the coupling could be understood by the rise and fall of the tails of the parallel electron velocity distribution functions on different flux surfaces at the same time. For typical LHCD experiments on EAST, the input power of the 4.6 GHz wave is dominant. Efforts are made aiming at studying the parameter regimes in which the power deposition profile of the 4.6 GHz wave can be modified by injecting a 2.45 GHz wave simultaneously. For the 4.6 GHz wave that can be Landau damping with electrons at far off-axis, if either the injected power at 2.45 GHz is comparable with that at 4.6 GHz or the incident $N_{||}$ of the 2.45 GHz wave reaches the high value (e.g., $5.7/\sqrt{T_{e,0}}$), the power deposition profile of the 4.6 GHz wave can be modified greatly due to the coupling with the 2.45 GHz wave. By combining these two approaches, it is shown that the power deposition profile of the 4.6 GHz wave can still be modified significantly when the 2.45 GHz wave is simultaneously injected with the parameters compatible with the ability of LH wave system on EAST. The simulated hard X-ray spectra are also given to demonstrate the synergy in near-axis region and the

reduction of fast electrons in off-axis region due to the coupling, respectively. Finally it is shown how a 4.6 GHz wave which cannot be Landau damped when injected alone is absorbed in low density plasmas with magnetic shear reversal configuration in the presence of a 2.45 GHz wave. Simulations shows that only 5% of the wave power at 4.6 GHz is deposited by Landau damping and a large fraction of wave power cannot be damped if it is injected alone. The simultaneous injection of a low power 2.45 GHz wave (about 25% of the injected power at 4.6 GHz) can improve the total power absorption of the 4.6 GHz wave to about 100%.

ACKNOWLEDGEMENTS

The authors appreciate the valuable discussion with Miao Hui Li in ASIPP for the LH systems on EAST. This work was supported by the program of National Key R&D Program of China under Grant No. 2017YFE0300400, the National Natural Science Foundation of China under Grant No. 11575239, the National ITER program of China under Contract No. 2015GB101003 and by an International Collaboration Grant No. DE-SC0010492 from the US Department of Energy. Numerical computations were performed at the ShenMa High Performance Computing Cluster at the Institute of Plasma Physics, at the Chinese Academy of Sciences.

REFERENCES

[1]N. J. Fisch, Physical Review Letters 41, 873 (1978).
[2]P. T. Bonoli, Physics of Plasmas 21, 061508 (2014).
[3]J. Hillairet, A. Ekedahl, M. Goniche, Y. S. Bae, J. Achard, A. Armitano, B. Beckett, J. Belo, G. Berger-By, J. M. Bernard, E. Corbel, L. Delpech, J. Decker, R. Dumont, D. Guilhem, G. T. Hoang, F. Kazarian, H. J. Kim, X. Litaudon, R. Magne, L. Marfisi, P. Mollard, W. Namkung, E. Nilsson, S. Park, Y. Peysson, M. Preynas, P. K. Sharma and M. Prou, Nuclear Fusion 53, 073004 (2013).
[4]C. Gormezano, A. C. C. Sips, T. C. Luce, S. Ide, A. Becoulet, X. Litaudon, A. Isayama, J. Hobirk, M. R. Wade, T. Oikawa, R. Prater, A. Zvonkov, B. Lloyd, T. Suzuki, E. Barbato, P. Bonoli, C. K. Phillips, V. Vdovin, E. Joffrin, T. Casper, J. Ferron, D. Mazon, D. Moreau, R. Bundy, C. Kessel, A. Fukuyama, N. Hayashi, F. Imbeaux, M. Murakami, A. R. Polevoi and H. E. S. John, Nuclear Fusion 47, S285 (2007).
[5]H. ITER Physics Expert Group on Energetic Particles, Current and Drive, Nuclear Fusion 39, 2495 (1999).
[6]X. Litaudon, R. Arslanbekov, G. T. Hoang, E. Joffrin, F. Kazarianvibert, D. Moreau, Y. Peysson, P. Bibet, P. Froissard and M. Goniche, Plasma Physics & Controlled Fusion 38, 1603 (1996).

[7]S. Ide, T. Fujita, O. Naito and M. Seki, Plasma Physics & Controlled Fusion 38, 1645 (1996).
[8]A. M. Garofalo, X. Z. Gong, J. Qian, J. Chen, G. Li, K. Li, M. H. Li, X. Zhai, P. Bonoli, D. Brower, L. Cao, L. Cui, S. Ding, W. X. Ding, W. Guo, C. Holcomb, J. Huang, A. Hyatt, M. Lanctot, L. L. Lao, H. Liu, B. Lyu, J. McClenaghan, Y. Peysson, Q. Ren, S. Shiraiwa, W. Solomon, Q. Zang and B. Wan, Nuclear Fusion 57, 076037 (2017).
[9]G. Giruzzi, J. F. Artaud, R. J. Dumont, F. Imbeaux, P. Bibet, G. Berger-By, F. Bouquey, J. Clary, C. Darbos, A. Ekedahl, G. T. Hoang, M. Lennholm, P. Maget, R. Magne, J. L. Segui, A. Bruschi and G. Granucci, Physical Review Letters 93 (2004).
[10]I. Fidone, G. Giruzzi, V. Krivenski, E. Mazzucato and L. F. Ziebell, Nuclear Fusion 27, 579 (1987).
[11]M. Shoucri, I. Shkarofsky, V. Fuchs, K. Kupfer, A. Bers and S. Luckhardt, Computer Physics Communications 55, 253 (1989).
[12]R. Dumont, G. Giruzzi and E. Barbato, Physics of Plasmas 7, 4972 (2000).
[13]R. J. Dumont and G. Giruzzi, Physics of Plasmas 11, 3449 (2004).
[14]Y. Yang, N. Xiang and Y. M. Hu, Physics of Plasmas 24, 082503 (2017).
[15]S. Ide, O. Naito, T. Kondoh, Y. Ikeda and K. Ushigusa, Phys Rev Lett 73, 2312 (1994).
[16]F. X. Soldner, F. Leuterer, R. Bartiromo, S. Bernabei, R. Buchse, O. Gehre, R. W. Harvey, M. Kornherr, K. Mccormick and H. D. Murmann, Nuclear Fusion 34, 985 (1994).
[17]M. Sakamoto, S. Itoh, K. N. Sato, K. Nakamura, H. Zushi, K. Hanada, E. Jotaki, K. Makino, S. Kawasaki and H. Nakashima, Nuclear Fusion 40, 453 (2000).
[18]W. Mao, D. Bojiang, X. Handong, Z. Lianmin, L. Liang, L. Shiyao, X. Ping, S. Youwen, H. Huaichuan and Y. Yong, Plasma Science & Technology 11, 534 (2009).
[19]S. J. Karttunen, T. J. H. Pättikangas, R. R. E. Salomaa, M. Shoucri, I. Shkarofsky, P. Bertrand and A. Ghizzo, Physica Scripta 60, 356 (1999).
[20]Y. Yang, N. Xiang and Y. M. Hu, Physics of Plasmas 24, 032502 (2017).
[21]S. Shiraiwa, G. Baek, P. T. Bonoli, I. C. Faust, A. E. Hubbard, O. Meneghini, R. R. Parker, G. M. Wallace, J. R. Wilson, R. W. Harvey, A. P. Smirnov, D. Brunner, B. LaBombard, C. Lau, R. Mumgaard, S. Scott, N. Tsujii and S. Wolfe, Nuclear Fusion 53, 113028 (2013).
[22]X. M. Zhai, N. Xiang, J. L. Chen, P. T. Bonoli, S. Shiraiwa, A. M. Garofalo, C. Yang, M. H. Li, J. P. Qian, G. Q. Li, K. Li, H. Q. Liu, B. Lyu and Q. Zang, Plasma Physics and Controlled Fusion 61, 045002 (2019).
[23]H. Takahashi, Physics of Plasmas 1, 2254 (1994).
[24]F. Paoletti, D. W. Ignat, J. Kesner, S. Bernabei, R. Kaita, B. Leblanc, F. M. Levinton and S. C. Luckhardt, Nuclear Fusion 34, 771 (1994).
[25]A. R. Esterkin and A. D. Piliya, Plasma Physics and Controlled Fusion 34, 1957 (1992).
[26]T. H. Stix, *Waves in plasmas*. (American Institute of Physics, New York, 1992).
[27]Y. Peysson, J. Decker, E. Nilsson, J. F. Artaud, A. Ekedahl, M. Goniche, J. Hillairet, B. Ding, M. Li, P. T. Bonoli, S. Shiraiwa and M. Madi, Plasma Physics and Controlled Fusion 58, 044008 (2016).
[28]C. Yang, P. T. Bonoli, J. C. Wright, B. J. Ding, R. Parker, S. Shiraiwa and M. H. Li, Plasma Physics and Controlled Fusion 56, 125003 (16 pp.) (2014).
[29]H. Du, S. Ding, J. Chen, Y. Wang, L. Hui, G. Xu, X. Zhai, H. Liu, Q. Zang and L. Bo, Nuclear Fusion 58, 066011 (2018).
[30]P. Bonoli, Physics of Plasmas 15, 1511 (2008).

[31]A. Schmidt, P. T. Bonoli, O. Meneghini, R. R. Parker, M. Porkolab, S. Shiraiwa, G. Wallace, J. C. Wright, R. W. Harvey and J. R. Wilson, Physics of Plasmas 18, 056122 (2011).
[32]W. Lu, S.-Y. Chen, C.-J. Tang, X.-Y. Bai, X.-J. Zhang and Y.-J. Hu, Chinese Physics Letters 30, 065203 (2013).
[33]P. Bonoli, IEEE Transactions on Plasma Science PS-12, 95 (1984).